

Lec. 4 Principles of signal digitization. Signal sampling

Signal digitization as general quantization of signal space

Practical solution - two step digitization: Discretization: conversion continuous signals into discrete signals (sets of numbers) & Element-wise quantization: rounding off those numbers to certain fixed (quantized) levels.

Principles of signal discretization. Signal discretization: signal expansion over a set of basis functions

Classification of discretization basis functions: shift (convolution), scale (multiplicative); combined shift&scale (multi-resolution) bases

Shift bases: rectangular function, sinc-function. Duality between rectangular and sinc-function bases. Piece-wise constant and band-limited signal approximation

Scale bases: Fourier series signal expansion; Walsh functions.

Combined shift&scale (multi-resolution) bases. Haar basis functions.

Optimal bases. RMS reconstruction error optimality. Karhunen-Loewe expansion and image correlation function computed over image statistical ensemble or data base.

Two-dimensional and multi-dimensional bases. Separable and inseparable bases. Discretization in computed tomography.

Image sampling

1-D sampling theorem. Sampling and periodical extension of signal Fourier spectrum. Optimality of the sinc-function sampling raster. Signal discretization and dimensionality of the signal space

Sampling 2-D and multi-dimensional signals. Rectangular, rotated rectangular and hexagonal discretization rasters.

Image sampling artifacts. Strobe-effect; moire-effect; pixellation effect.

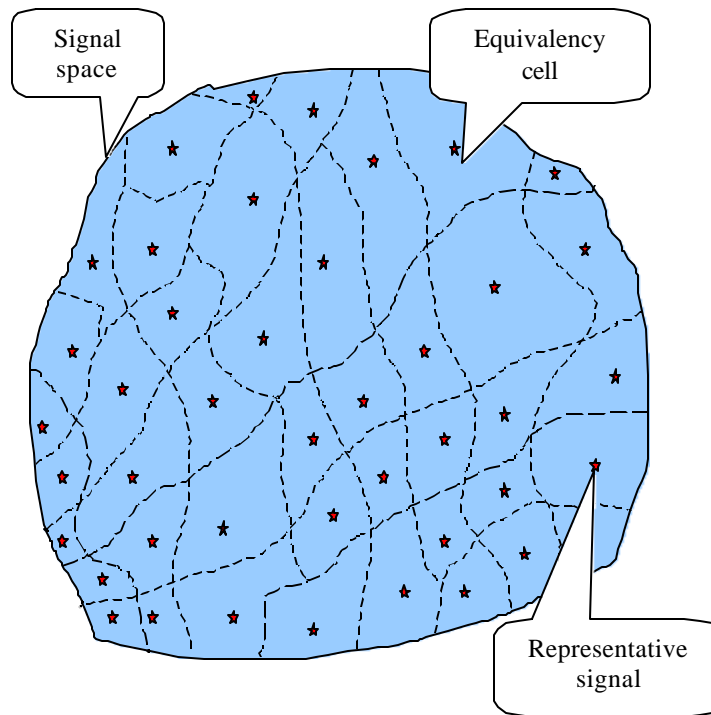
Sub-band signal decomposition and “multi-resolution” signal sampling

4.1 General quantization of signal space :

- splitting signal space into a set of equivalency cells
- assigning to signals a digital index of the cell they belong to

Signal reconstruction from its digital representation:

- Given signal's digital index, generating representative signal of the cell with this index



The dimensionality of image signal space is tremendous. For instance, for images stored in modern computers: $\gg 256^{3 \cdot 1200 \cdot 780}$.

Practical solution - two step digitization:

- Discretization: conversion continuous signals into discrete signals (sets of numbers)
- Element-wise quantization: rounding off those numbers to certain fixed (quantized) levels.

4.2 Principles of Signal discretization

A commonly accepted option for signal discretization: signal expansion over a set of basis functions:

Discretization:

$$\mathbf{a}_k = \int_x a(x) \mathbf{j}_k^{(d)}(x) dx \quad (4.1)$$

where $\{\mathbf{j}_k^{(d)}(x)\}$ are discretization basis functions. They are implemented as sensor aperture functions. k is basis function index, $k = 0, \dots, N - 1$. N is amount of basis functions. Set of numbers $\{\mathbf{a}_k\}$ form *signal's discrete representation*.

Signal reconstruction from its discrete representation:

$$a(x) \gg \tilde{a}(x) = \sum_{k=0}^{N-1} \hat{\mathbf{a}}_k \mathbf{j}_k^{(r)}(x), \quad (4.2)$$

where $\{\mathbf{j}_k^{(r)}(x)\}$ is a set of reconstruction basis functions. They are implemented as image display aperture functions. The reconstruction is always approximate.

Requirements to discretization/reconstruction basis functions:

- Minimization of the signal reconstruction (Eq. 4.2) error
- Easiness of implementation

4.3 Classification of discretization basis functions.

Main principle: all functions in the set are generated from one basis function by its certain modification.

4.3.1 Coordinate shift as a building operation: $\{j_k(x) = j(x - kDx)\}$

Two major examples of shift basis function:
Rectangular impulse functions

$$j_k(x) = \text{rect}_{\frac{Dx}{2}} \frac{x - kDx}{Dx} \quad (4.3)$$

where

$$\text{rect}(x) = \begin{cases} 1, & 0 \leq x < 1 \\ 0, & \text{otherwise} \end{cases} \quad (4.4)$$

and sinc-functions

$$j_k(x) = \text{sinc}_{\frac{Dx}{2}} \frac{x - kDx}{Dx} \quad (4.5)$$

where

$$\text{sinc}(x) = \frac{\sin x}{x} \quad (4.6)$$

Rectangular impulse basis functions are orthogonal. For rectangular impulse basis functions

$$j_k^{(r)}(x) = \frac{1}{Dx} \text{rect}_{\frac{Dx}{2}} \frac{x - kDx}{Dx} \quad (4.7)$$

used as the discretization basis, signals are represented their mean values over discretization intervals:

$$a_k = \frac{1}{Dx} \int_{kDx}^{(k+1)Dx} a(x) \text{rect}_{\frac{Dx}{2}} \frac{x - kDx}{Dx} dx = \frac{1}{Dx} \int_{kDx}^{(k+1)Dx} a(x) dx = \overline{a(kDx)} \quad (4.8)$$

Reciprocal signal reconstruction basis in this case is composed of functions

$$j_k^{(r)}(x, k) = \text{rect}_{\frac{Dx}{2}} \frac{x - kDx}{Dx} \quad (4.9)$$

Signals reconstructed with this basis are piece-wise constant functions (Figure 4-1):

$$a(x) \approx \tilde{a}(x) = \sum_{k=0}^{N-1} a(kDx) \text{rect}_{\frac{Dx}{2}} \frac{x - kDx}{Dx} \quad (4.10)$$

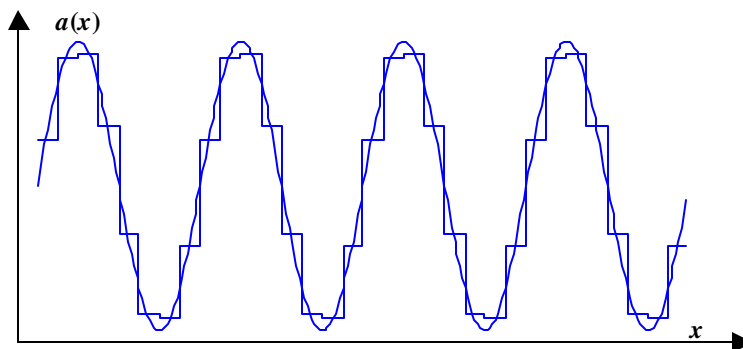


Figure 4-1. Continuous sinusoidal signal and its copy reconstructed after discretization with rectangle impulse discretization and reconstruction basis functions

Sinc- functions (sampling functions) are in a sense dual to rectangle impulse ones. As it follows from the equation:

$$\int_{-\infty}^{\infty} \text{rect}[(f + 1/2Dx)Dx] \exp(-i2\pi fx) dx = \int_{-1/2Dx}^{1/2Dx} \exp(-i2\pi fx) df = \frac{1}{Dx} \text{sinc}_{\frac{Dx}{2}} \frac{f}{Dx} \quad (4.11)$$

their Fourier spectrum is a rectangular impulse function (see Figure 4-2).

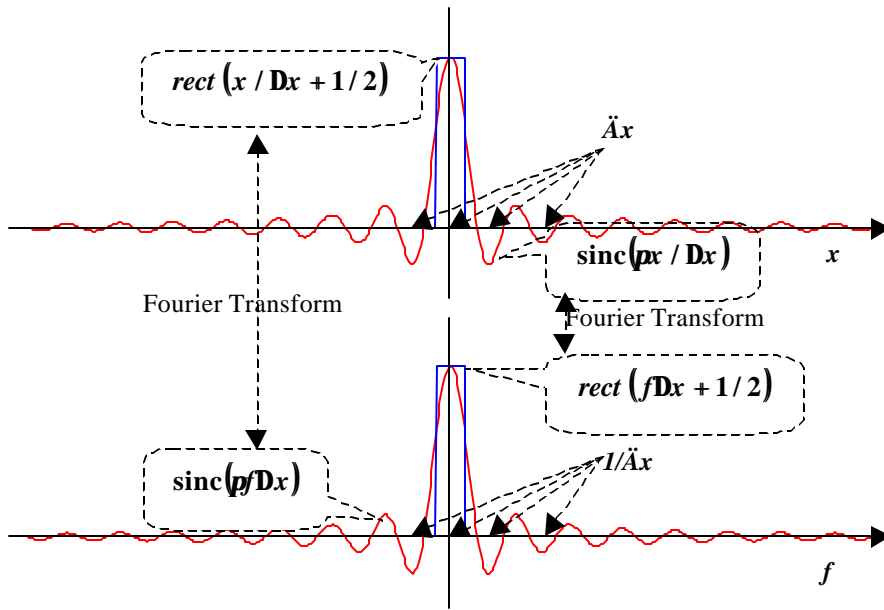


Figure 4-2. Duality of rectangular impulse and sinc basis functions

Sinc-functions $\frac{1}{Dx} \text{sinc}\left(\frac{x - kDx}{Dx}\right)$ are the discretization basis functions:

$$a_k = \frac{1}{Dx} \int_{-\infty}^{\infty} a(x) \text{sinc}\left(\frac{x - kDx}{Dx}\right) dx. \quad (4.12)$$

Using *shift theorem* and *convolution theorem* of the theory of Fourier Transform, one can show that sinc-functions are mutually orthogonal:

$$\frac{1}{Dx} \int_{-\infty}^{\infty} \text{sinc}\left(\frac{x - kDx}{Dx}\right) \text{sinc}\left(\frac{x - lDx}{Dx}\right) dx = \text{sinc}(p(k - l)) = d(k - l) = \begin{cases} 1, & k = l \\ 0, & k \neq l \end{cases} \quad (4.13)$$

Therefore functions $\frac{1}{Dx} \text{sinc}\left(\frac{x - kDx}{Dx}\right)$ are reconstruction functions for this basis:

$$a(x) \approx \tilde{a}(x) = \sum_{k=0}^{N-1} a_k \text{sinc}\left(\frac{x - kDx}{Dx}\right). \quad (4.14)$$

Because Fourier spectrum of functions $\frac{1}{Dx} \text{sinc}\left(\frac{x - kDx}{Dx}\right)$ is bounded in the range

$[-1/2Dx, 1/2Dx]$ (see Eq.4.11), basis composed of them generates signals that belong to the class of *band limited functions*. It also follows from Eq. (4.14) that coefficients $\{a_k\}$ of discrete representation of band limited functions are equal to functions' samples at equidistant points $\{x = kDx\}$:

$$a_k = \tilde{a}(kDx) \quad (4.15)$$

This is where the name "sampling functions" derives from.

Eqs. 4.10 and 4.14 can also be regarded as convolution $\text{conv}(\cdot, \cdot)$ of signals

$$\tilde{a}(x) = \sum_{k=0}^{N-1} a_k d(x - kDx) \quad (4.16)$$

with reconstruction basis functions:

$$\tilde{a}(x) = \text{conv}(\tilde{a}(x), j_d(x)) = \text{conv}\left(\sum_{k=0}^{N-1} a_k d(x - kDx), j_d(x)\right) = \sum_{k=0}^{N-1} a_k j_d(x - kDx). \quad (4.17)$$

This justifies yet another name for shift basis functions, the *convolution basis functions*, and treatment of Eq. (4.17) for reconstruction of continuous signals from their discrete representation as *convolution based interpolation*.

4.3.2 Coordinate scaling as a basis building operations: $scale\ basis\ functions\ j_k(x) = j(kx)$

Sinusoidal basis functions $\{\cos(2\pi kx / X)\}$ and $\{\sin(2\pi kx / X)\}$.

These functions are orthogonal. Functions $\{\cos(2\pi kx / X)\}$ when used as a reconstruction basis, reconstruct signals

$$a(x) \approx \tilde{a}^{(e)} = \sum_{k=0}^{N-1} \tilde{a}_k^{(e)} \cos(2\pi kx / X) \quad (4.18)$$

that are periodical, with period X , and even functions ($a(x) = a(-x)$).

Functions $\{\sin(2\pi kx / X)\}$ used as a reconstruction basis reconstruct signals

$$a(x) \approx \tilde{a}^{(s)} = \sum_{k=0}^{N-1} \tilde{a}_k^{(s)} \sin(2\pi kx / X) \quad (4.19)$$

that are also periodical, with period X , and odd functions ($a(x) = -a(-x)$). Signal representation coefficients for these bases are found, respectively, as,

$$\tilde{a}_k^{(e)} = \frac{1}{X} \int_{-X/2}^{X/2} a(x) \cos(2\pi kx / X) dx \quad (4.20)$$

$$\tilde{a}_k^{(s)} = \frac{1}{X} \int_{-X/2}^{X/2} a(x) \sin(2\pi kx / X) dx \quad (4.21)$$

In reality, signals are, in general, neither even nor odd functions. There are two ways to avoid this obstacle in using sinusoidal basis functions. One way is form, from signals taken at interval $[0, X]$, auxiliary even or odd signals defined on interval $[0, 2X]$ of double length as, respectively:

$$\tilde{a}^{(e)}(x) = \begin{cases} a(x), & 0 \leq x < X \\ a(2X - x), & X \leq x < 2X \end{cases} \quad (4.22)$$

and

$$\tilde{a}^{(s)}(x) = \begin{cases} a(x), & 0 \leq x < X \\ -a(2X - x), & X \leq x < 2X \end{cases} \quad (4.23)$$

With this signal “*symmetrization*”, bases $\{\cos(\pi kx / X)\}$ and $\{\sin(\pi kx / X)\}$ can be used for discretization and reconstruction of arbitrary signals. Signal representation coefficients should be computed in this case as, respectively,

$$\tilde{\tilde{a}}_k^{(e)} = \frac{1}{2X} \int_0^{2X} \tilde{a}^{(e)}(x) \cos(\pi kx / X) dx = \frac{1}{X} \int_0^X a(x) \cos(\pi kx / X) dx \quad (4.24)$$

$$\tilde{\tilde{a}}_k^{(s)} = \frac{1}{2X} \int_0^{2X} \tilde{a}^{(s)}(x) \sin(\pi kx / X) dx = \frac{1}{X} \int_0^X a(x) \sin(\pi kx / X) dx \quad (4.25)$$

and signals should be reconstructed from their discrete representations $\{\tilde{\tilde{a}}_k^{(e)}\}$ and $\{\tilde{\tilde{a}}_k^{(s)}\}$ as, respectively,

$$a(x) \approx \tilde{a} = \sum_{k=0}^{N-1} \tilde{\tilde{a}}_k^{(e)} \cos(\pi kx / X) \quad (4.26)$$

or

$$a(x) \approx \tilde{a} = \sum_{k=0}^{N-1} \tilde{\tilde{a}}_k^{(s)} \sin(\pi kx / X) \quad (4.27)$$

The second way to avoid the above mentioned limitations of sinusoidal basis functions $\{\cos(2\pi kx / X)\}$ and $\{\sin(2\pi kx / X)\}$ is to use them in combination:

$$a(x) = \sum_{k=0}^{N-1} \tilde{a}_k^{(e)} \cos(2\pi kx / X) + \sum_{k=0}^{N-1} \tilde{a}_k^{(s)} \sin(2\pi kx / X), \quad (4.28)$$

where the representation coefficients $\{\tilde{a}_k^{(e)}\}$ and $\{\tilde{a}_k^{(s)}\}$ are defined by Eqs. (4.20) and (4.21).

All these methods of signal expansion over set of sinusoidal basis functions are different versions of Fourier series expansion of a signal in the interval of the length X . Mathematical treatment of Fourier series expansion is much simplified if pairs of functions $\{\cos(2\pi kx / X)\}$ and $\{\sin(2\pi kx / X)\}$ are replaced by a complex exponential basis functions $\{\exp(i2\pi kx / X)\}$:

$$a(x) = \sum_k \hat{a}_k \exp(i2\pi kx / X) \quad (4.29)$$

where coefficients $\{\hat{a}_k\}$ are complex numbers:

$$\hat{a}_k = \frac{1}{X} \int_{-X/2}^{X/2} \hat{a}(x) \exp(-i2\pi kx / X) dx \quad (4.30)$$

Walsh functions

For basis of exponential functions $\{\exp(i2\pi kx / X)\}$, generating basis functions by scaling their argument can be treated also as generating by means of multiplying mother function:

$$\exp(i2\pi kx / X) = \prod_{l=1}^k \exp(i2\pi l / X) \quad (4.31)$$

There exists yet another family of orthogonal functions built with the same principle, **Walsh functions**. Walsh functions assume only two values; either 1, or -1. They are generated by multiplication of clipped sinusoidal functions called the **Rademacher functions**

$$rad_k(x) = \text{sign}(\sin(2^k \pi x / X)) \quad (4.32)$$

Any two Rademacher functions are mutually orthogonal. However, the system of functions $\{rad_k(x)\}$ is incomplete in the same sense as families of functions $\{\cos(2\pi kx / X)\}$ and $\{\sin(2\pi kx / X)\}$ are incomplete. The Walsh functions are an extension of Rademacher functions to a complete system. They are defined as

$$wal_k(x) = \prod_{m=0}^{k_m^{GC}} rad_{m+1}(x) \quad (4.33)$$

where k_m^{GC} is the m -th digit of the so-called Gray code of number k . Gray code digits are generated from digits $\{k_m\}$ of binary representation of the number

$$k = \sum_{m=0}^{\infty} k_m 2^m; \quad k_m = 0,1 \quad (4.34)$$

according to the following rule:

$$k_m^{GC} = k_m \hat{\mathbf{A}} k_{m+1}, \quad (4.35)$$

where $\hat{\mathbf{A}}$ stands for modulo 2 addition.

Formula (3.2.34) reveals the origin of the Walsh functions. However, for the purpose of calculating their values another representation of the Walsh functions::

$$wal_k(\mathbf{x}) = \prod_{m=0}^{\infty} [(-1)^{x_{m+1}}]^{k_m^{GC}} = (-1)_{m=0}^{\sum_{m=0}^{\infty} k_m^{GC} x_{m+1}} \quad (4.36)$$

is useful, where

$$\mathbf{x} = x / X = \sum_{m=0}^{\infty} x_m 2^{-m}; \quad x_0 = 0; \quad x_{m>0} = 0,1 \quad (4.37)$$

The Walsh functions are orthogonal on the interval $[0, X]$. Because of their origin as a product of Rademacher functions, multiplication of two Walsh functions results in another Walsh function with shifted an index or argument. The shift, called **dyadic shift**, is determined through the bit-by-bit modulo 2 addition of functions' indices or, respectively, arguments:

$$wal_k(\mathbf{x}) wal_l(\mathbf{x}) = wal_{k \hat{\mathbf{A}} l}(\mathbf{x}); \quad (4.38)$$

$$wal_k(\mathbf{x}) wal_k(\mathbf{z}) = wal_k(\mathbf{x} \hat{\mathbf{A}} \mathbf{z}) \quad (4.39)$$

One can regard $\sum_{m=0}^{\infty} k_m^{GC} x_{m+1}$ in the definition of Walsh as a scalar product of vectors $\{k_m^{GC}\}$ and $\{x_{m+1}\}$. In this sense one can treat basis of Walsh functions as a scale basis. Multiplicative nature of Walsh functions and exponential ones justifies yet another name for these families of bases, multiplicative bases.

Walsh function are akin to complex exponential functions $\{\exp(i2\pi kx / X)\}$ in one more respect. This can be seen if (-1) in Eq. (4.36) is replaced by $\exp(ip)$:

$$wal_k(\mathbf{x}) = \exp\left\{i p \sum_{m=0}^{\infty} k_m^{GC} x_{m+1} \frac{\pi}{\theta}\right\} \quad (4.40)$$

and from comparison of graphs of sinusoidal and Walsh functions shown in figure 3-4

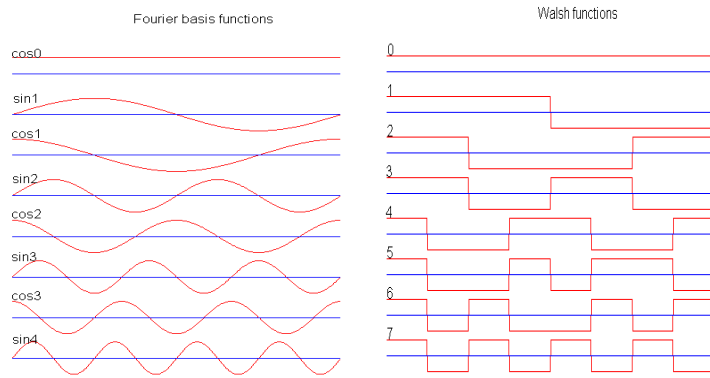


Figure 4-3. Sinusoidal and Walsh functions

As one can see from the figure, an important parameter that unites both families of functions is the number of zero crossing which coincides, for these functions, with their index k . As it was mentioned above, for sinusoidal functions, this parameter has an association with the notion of frequency. For Walsh functions, this parameter obtained name of “sequency”.

Sequency wise ordering of Walsh functions is not accidental. In principle, ordering basis functions can be arbitrary; the only condition one should obey is matching between signal representation coefficients $\{a_k\}$ and discretization and reconstruction basis functions $\{j_k^{(d)}(x)\}$ and $\{j_k^{(r)}(x)\}$. However almost always natural ways of natural ordering exist. For instance, for shift (convolution) bases the natural ordering is according to successive coordinate shifts. Sinusoidal basis functions are naturally ordered in frequency of signal Fourier transform. This why sequence (number of zero crossing) wise ordering of Walsh functions can also be regarded natural.

However, the advantage of such an ordering is more fundamental. The most natural requirement to ordering basis functions for signal representation is the ordering for which signal approximation error for finite number N of terms in signal expansion over the basis monotonically decreases with the growth of N . For Walsh functions, it happens that, for conventional analog signals, sequency wise ordering satisfies this requirement much better than other methods of ordering. Figure 3-5 illustrates this feature of Walsh function signal spectra. Graphs on the figure show averaged squared Walsh spectral coefficients of image rows as functions of coefficients’ indices for sequency wise (Walsh) ordering (left) and for Hadamard ordering (right). In Hadamard ordering, digits $\{k_m\}$ of binary representation of index k (3.2.35) rather than digits $\{k_m^{GC}\}$ are used for generating Walsh functions:

$$walhad_k(x) = (-1)^{\sum_{m=0}^{\infty} k_m x_{m+1}} \quad (4.41)$$

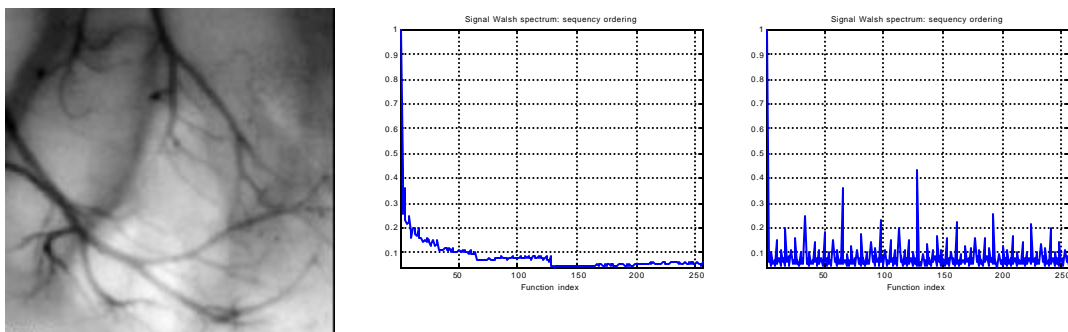


Figure 4-4. Comparison of image Walsh function spectra in Walsh (left) and Hadamard (right) ordering

Signal expansion over Walsh function basis approximates signals with piecewise functions just as it is the case for rectangle impulse basis functions.

4.3.3 Combination of shift and scale: Wavelets bases

A distinctive feature of shift (convolution) bases is that, for them, signal representation coefficients depend on signal values in the vicinity of the corresponding sampling point, and therefore they carry local information about signals. In contrast to them, signal discrete representation for scale (multiplicative) bases is “global”: signal representation coefficients depend on the entire signal. Sometimes it is useful to have a combination of these two features in the signal discrete representation. This is achieved with wavelet basis functions built using a combination of shift and scaling of a mother function. A most immediate example of such a combination are **Haar functions**. Haar functions are generated from shift basis of rectangle impulse functions $\{rect(x - kDx / Dx)\}$ and Rademacher functions $\{sign(\sin(2^k \pi x / X))\}$ in the following way:

$$har_k(x) = 2^m rad_{\widehat{m}}(x) rect_{\frac{x}{X}} \left(2^m \frac{x}{X} - [k] \bmod 2^m \right), \quad (4.42)$$

where \widehat{m} is index of the most significant non-zero digit (bit) in binary representation of k (Eq. (3.2.35)) and $[k] \bmod 2^m$ is residual from division of k by 2^m .

The Haar functions are orthonormal on the interval $[0, X]$. Graphs of first eight Haar functions are shown in Fig. 4-4.

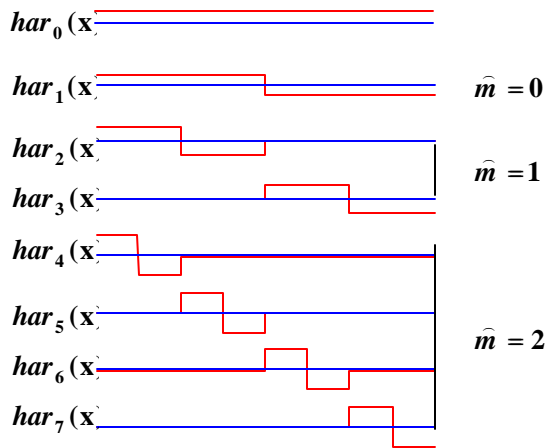


Figure 4-4. First eight Haar functions

One can see from the figure, that Haar functions form groups in scale and that functions within each group are generated by shift in coordinates with shift interval coordinated with the scale. One can also see that signals reconstructed from their discrete representation over Haar basis functions belong to the same family of piece-wise constant functions as signals reconstructed in the base of rectangle impulse basis functions.

Numerical values of Haar functions may be found at each point by expressing them, as in the case of Walsh functions, via a binary code argument representations (4.34 and 37):

$$har_k(x) = 2^m (-1)^{d(\lfloor \frac{x}{X} \rfloor - (k) \bmod 2^m)}. \quad (4.43)$$

At present time, numerous other wavelet bases are known.

4.4 Optimality of bases. Karhunen-Loeve Transform

In this section, we address the problem of optimality of bases in terms of the accuracy of signal approximation with a limited number of terms in their expansion over the bases. For generality, we will assume that signals belong to a certain family (ensemble) of signals and that the accuracy of signal representation is evaluated on average over this family.

Let $\{a(x, \mathbf{w})\}$ be a set (in terms of a parameter $\mathbf{w} \in \mathbf{W}$) of signals to be represented by their approximations in a form of finite expansions:

$$a(x, \mathbf{w}) \approx \tilde{a}(x, \mathbf{w}) = \sum_{k=0}^{N-1} \tilde{a}_k(\mathbf{w}) j_k(x) \quad (4.44)$$

over orthonormal basis functions $\{j_k(x)\}$ such that

$$\int_x j_k(x) j_l^*(x) dx = d(k, l) = 0^{k \neq l}. \quad (4.45)$$

Let also evaluate the approximation accuracy in terms of mean squared approximation error (MSE):

$$|\mathbf{e}(\mathbf{w})|^2 = \int_X |a(x, \mathbf{w}) - \tilde{a}(x, \mathbf{w})|^2 dx = \int_X \left| a(x, \mathbf{w}) - \sum_{k=0}^{N-1} \hat{\mathbf{a}}_k(\mathbf{w}) j_k(x) \right|^2 dx \quad (4.46)$$

Optimal values of $\{\hat{\mathbf{a}}_k(\mathbf{w})\}$ that minimize MSE can be found by equating to zero derivatives of Eq. (4.46) over $\{\hat{\mathbf{a}}_k(\mathbf{w})\}$:

$$\frac{\partial}{\partial \hat{\mathbf{a}}_k(\mathbf{w})} \int_X \left| a(x, \mathbf{w}) - \sum_{k=0}^{N-1} \hat{\mathbf{a}}_k(\mathbf{w}) j_k(x) \right|^2 dx = 0, \quad (4.47)$$

from which one can obtain:

$$\hat{\mathbf{a}}_k(\mathbf{w}) = \int_X a(x, \mathbf{w}) j_k^*(x) dx, \quad (4.48)$$

where * stands for a complex conjugate.

From Eq. (4.47) it follows that minimal MSE is equal to

$$|\mathbf{e}(\mathbf{w})|_{\min}^2 = \int_X |a(x, \mathbf{w})|^2 dx - \sum_{k=0}^{N-1} |\hat{\mathbf{a}}_k(\mathbf{w})|^2 \quad (4.49)$$

By an appropriate selection of bases functions $\{j_k(x)\}$ one can further minimize average MSE over the given set \mathbf{W} of signals as defined by parameter \mathbf{w} :

$$\begin{aligned} \{j_k(x)\}_{opt} &= \arg \min_{\{j_k(x)\}} \int_{\mathbf{W}} AV_{\mathbf{w}} \int_X |a(x, \mathbf{w})|^2 dx - \sum_{k=0}^{N-1} |\hat{\mathbf{a}}_k(\mathbf{w})|^2 \\ \arg \min_{\{j_k(x)\}} \int_{\mathbf{W}} AV_{\mathbf{w}} \int_X |a(x, \mathbf{w})|^2 dx - \sum_{k=0}^{N-1} AV_{\mathbf{w}} \int_X |\hat{\mathbf{a}}_k(\mathbf{w})|^2 &= \arg \max_{\{j_k(x)\}} \int_{\mathbf{W}} AV_{\mathbf{w}} \sum_{k=0}^{N-1} |\hat{\mathbf{a}}_k(\mathbf{w})|^2 \\ \arg \max_{\{j_k(x)\}} \int_{\mathbf{W}} AV_{\mathbf{w}} \sum_{k=0}^{N-1} \int_X a(x, \mathbf{w}) a^*(y, \mathbf{w}) j_k^*(x) j_k(y) dx dy &= \\ \arg \max_{\{j_k(x)\}} \int_{\mathbf{W}} AV_{\mathbf{w}} \sum_{k=0}^{N-1} \int_X \int_X a(x, \mathbf{w}) a^*(y, \mathbf{w}) j_k^*(x) j_k(y) dx dy &= \\ \arg \max_{\{j_k(x)\}} \int_{\mathbf{W}} AV_{\mathbf{w}} \sum_{k=0}^{N-1} R_a(x, y) j_k^*(x) j_k(y) dx dy &= \end{aligned} \quad (4.50)$$

where $AV_{\mathbf{w}}$ means averaging over the signal set \mathbf{W} . Function $R_a(x, y)$

$$R_a(x, y) = AV_{\mathbf{w}} (a(x, \mathbf{w}) a^*(y, \mathbf{w})) \quad (4.51)$$

is called “correlation function” of the set of signals $\{a(x, \mathbf{w})\}$. Denote

$$RF(x) = \int_X R_a(x, y) j_k(y) dy \quad (4.52)$$

Then optimal bases functions $\{j_k(x)\}$ are found from

$$\{j_k(x)\} = \arg \max_{\{j_k(x)\}} \int_{\mathbf{W}} AV_{\mathbf{w}} \int_X RF(x) j_k^*(x) dx \quad (4.53)$$

From Cauchy-Schwarz-Buniakowsky inequality

$$\int_X f_1(x) f_2^*(x) dx \leq \left(\int_X |f_1(x)|^2 dx \right)^{1/2} \left(\int_X |f_2(x)|^2 dx \right)^{1/2} \quad (4.54)$$

it follows that solution of Eq. (4.53) is

$$RF(x) = \int_X R_a(x, y) j_k(y) dy = I j_k(x) \quad (4.55)$$

This means that optimal bases functions are eigen functions of integral equation Eq.(3.2.55) with kernel defined by the correlation function (3.2.51) of the set of signals ([10,11]). Such bases are called **Karhunen-Loeve bases**.

An important special case is that of signals with correlation function that depends only on the difference of its arguments:

$$R_a(x, y) = R_a(x - y) \quad (4.56)$$

In this case the basis optimality condition takes the form:

$$\int_{-\infty}^{\infty} \hat{R}_a(x-y) \mathbf{j}(y, f) dy = \mathbf{I}(f) \mathbf{j}^*(x, f). \quad (4.57)$$

This condition is satisfied with exponential basis functions

$$\mathbf{j}(x, f) = \exp(i2\pi f x). \quad (4.58)$$

Two important conclusions follow from this result:

- Integral Fourier transform is an MSE optimal Karhunen-Loeve transform for signals with correlation function that depends only on difference of its arguments;
- The best, in MSE sense, approximation of such signals is their approximation with functions whose Fourier spectrum is equal to zero outside a certain bandwidth $[-F, F]$ (**band limited functions**):

$$\tilde{a}(x, \mathbf{w}) = \int_{-F}^F \hat{a}(f, \mathbf{w}) \mathbf{j}(x, f) df. \quad (4.59)$$

that defines minimal approximation MSE:

$$\left[AV_{\mathbf{w}} |e(\mathbf{w})|^2 \right]_{\min} = \int_{-F}^F AV_{\mathbf{w}} \{ |a(f, \mathbf{w})|^2 \} df + \int_{-F}^F AV_{\mathbf{w}} \{ |a(f, \mathbf{w})|^2 \} df \quad (4.60)$$

4.5 Two dimensional and multi dimensional bases

Two-dimensional and multi-dimensional basis functions are most frequently (although not always) generated as separable functions of two variables by the product of two one-dimensional ones. The underlying reason is the easiness of hardware and software generating the basis functions and lower computational complexity of computing signal representation coefficients. In the case of separable basis functions, which are the product of two one-dimensional functions, the job of evaluating of a scalar product is reduced to performing two one-dimensional summations rather than one two-dimensional:

$$\mathbf{a}_{r,s} = \prod_{k=0}^{N_1-1} \prod_{l=0}^{N_2-1} \hat{a}_{k,l} \mathbf{j}_{r,s}^{(d)}(k, l) = \prod_{k=0}^{N_1-1} \hat{a}_{k,l} \mathbf{j}_r^{(d1)}(k) \mathbf{j}_s^{(d2)}(l) = \prod_{k=0}^{N_1-1} \hat{a}_{k,l} \mathbf{j}_s^{(d2)}(l) \prod_{l=0}^{N_2-1} \hat{a}_{k,l} \mathbf{j}_r^{(d1)}(k) \quad (4.61)$$

As one can see from Eq. 4.61, direct computation of 2-D sum requires $N_1^2 N_2^2$ multiplication/summation operations while two separable 1-D summations require $N_1 N_2 (N_1 + N_2)$ operations. For large 2-D arrays, saving is very substantial. Note that in separable two- and multi-dimensional bases multiplicand 1-D basis functions are not necessarily should be identical, though most frequently they are.

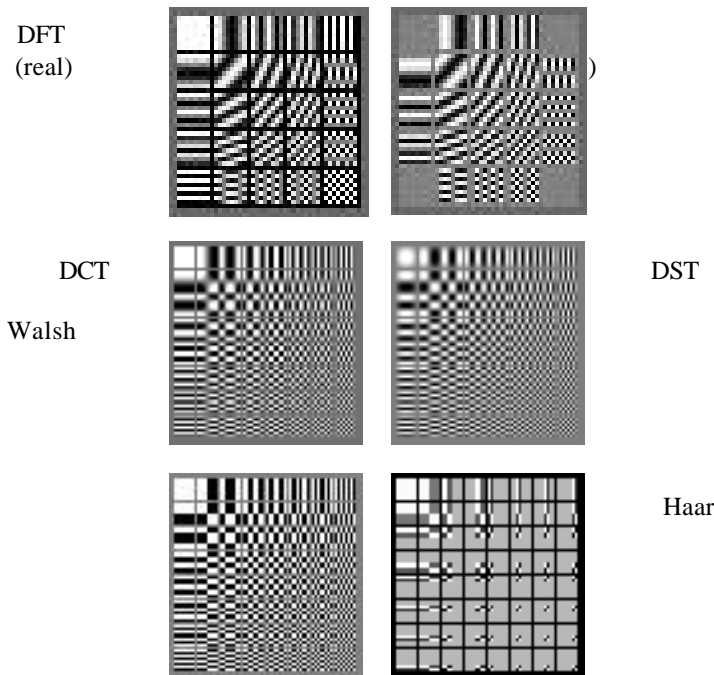


Figure 4-5. Examples of 8x8 sets of 2-D basis functions for DFT, DST, Walsh and Haar transforms displayed as images

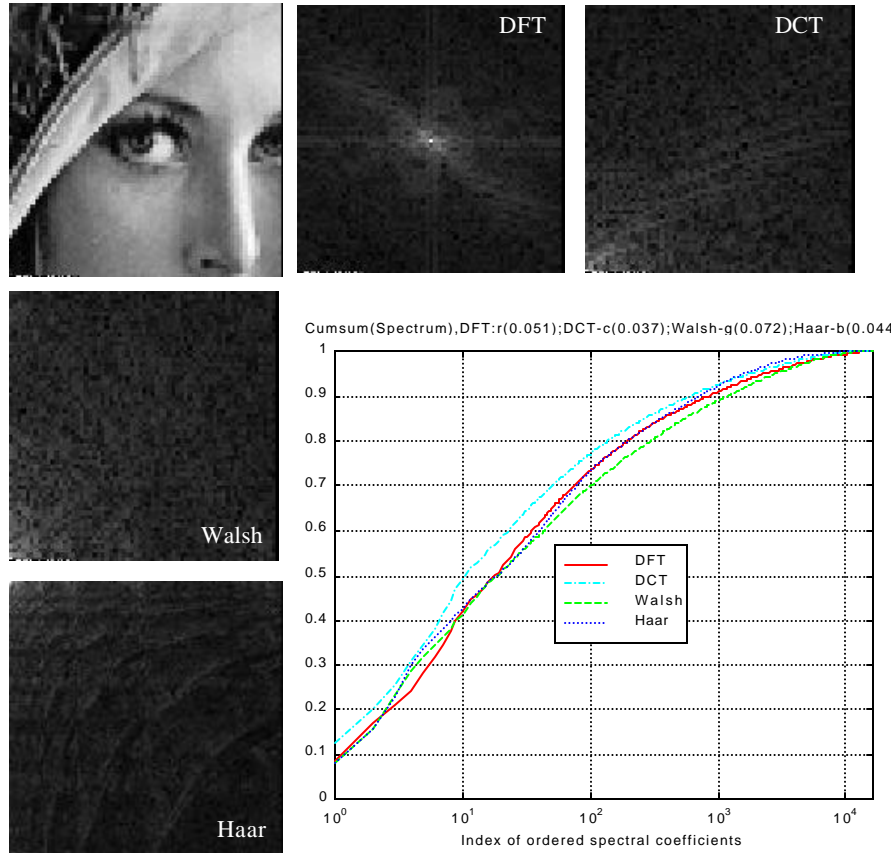


Figure 4-6. Comparison of image DFT, DCT, Walsh and Haar spectra. Graph illustrates the speed with which magnitude wise sorted spectral coefficients converge to the entire image signal energy.

4.6 Image sampling

4.6.1 1-D sampling theorem

The most widely used method for signal/image discretization is signal/image *sampling* by sensing them with a set of sensors that are equidistantly placed in signal/image coordinates. The sampling is carried out either by a mechanical or electronic signal/image scanning with a single sensor or with an array of sensors that work in parallel. The latter is exemplified by modern CCD and CMOS TV cameras. Remarkable enough that image sampling was first invented by the Nature in a form of a compound and retinal eyes

Signal sampling can mathematically be treated as signal representation over shifted bases. Let $\mathbf{j}_r(\mathbf{x})$ be a point spread function of a signal/image reconstruction/display device and $\mathbf{j}_d(\mathbf{x})$ be a point spread function of a signal discretization device given in the same measurement units. Then discrete representation of a signal $\mathbf{a}(\mathbf{x})$ over a basis generated by shifts of the discretization device point spread function by multiple of the discretization interval $\mathbf{D}\mathbf{x}$ is:

$$\mathbf{a}_k = \int_x \mathbf{a}(\mathbf{x}) \mathbf{j}_d(\mathbf{x} - k\mathbf{D}\mathbf{x}) d\mathbf{x}, \quad (4.6.1a)$$

and its reconstruction over basis formed by the corresponding shifts of point spread function of the reconstruction device is

$$\mathbf{a}(\mathbf{x}) \approx \mathbf{a}_r(\mathbf{x}) = \sum_k \mathbf{a}_k \mathbf{j}_r(\mathbf{x} - k\mathbf{D}\mathbf{x}). \quad (4.6.1b)$$

Integration over x in Eq. 4.6.1a and summation over k in Eq.4.6.1b are performed within signal boundaries.

Although usually signals are finite functions, mathematical analysis of the discretization by sampling is much simplified if one assumes that signals are infinite and integer index k of shift bases functions also runs in infinite limits:

$$\mathbf{a}_k = \int_{-\infty}^{\infty} a(x) \mathbf{j}_d(x - kDx) dx \quad (4.6.2a)$$

$$a(x) \approx a_r(x) = \sum_{k=-\infty}^{\infty} \mathbf{a}_k \mathbf{j}_r(x - kDx) \quad (4.6.2b)$$

Eq.(4.6.2a) means that coefficients $\{\mathbf{a}_k\}$ of signal discrete representation over shift basis functions $\{\mathbf{j}_d(x - kDx); \mathbf{j}_r(x - kDx)\}$ are equidistant samples

$$\mathbf{a}_k = a_{df}(kDx) = \int_{-\infty}^{\infty} a_{df}(x) \mathbf{d}(x - kDx) dx \quad (4.6.3)$$

of signal $a_{df}(x)$

$$a_{df}(x) = \int_{-\infty}^{\infty} a(\mathbf{x}) \mathbf{j}_d(x - \mathbf{x}) d\mathbf{x} \quad (4.6.3)$$

obtained from signal $a(x)$ by its convolution with a point spread function of the discretization device. A model of the discretization device that corresponds to such a representation is shown in Fig. 4-7.

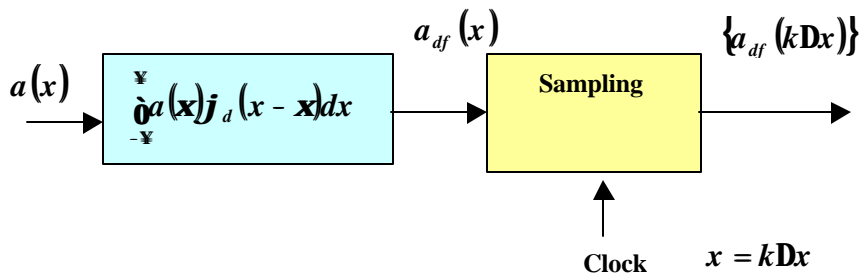


Figure 4-7. Mathematical model of the sampling device

Signal reconstruction from its sampled representation described by Eq. (4.6.1a) can, in its turn, be also regarded as filtering a discrete signal

$$\tilde{a}(x) = \sum_{k=-\infty}^{\infty} \mathbf{a}_k a_{df}(kDx) \mathbf{d}(x - kDx) \quad (4.6.4)$$

with a filter whose impulse response is equal to point spread function $\mathbf{j}_r(x)$ of the signal reconstruction device:

$$a_r(x) = \int_{-\infty}^{\infty} \tilde{a}(\mathbf{x}) \mathbf{j}_r(x - \mathbf{x}) d\mathbf{x} \quad (4.6.5)$$

as it is illustrated by the flow diagram in Fig. 4-8.

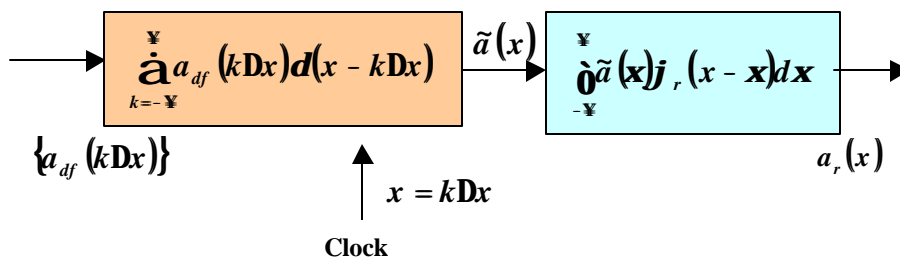


Figure 4-8. Mathematical model of the device for restoring continuous signals from their samples

Further analysis of signal sampling is much simplified in Fourier Transform domain. Compute Fourier Transforms of signals $a(x)$, $a_r(x)$, $a_{df}(f)$ and $\tilde{a}(x)$

$$a(f) \circledast a_r(f) = \sum_{k=-\infty}^{\infty} \hat{a}_k a_r \exp(i2\pi k f \Delta x) \overset{\text{DFT}}{\underset{\text{IDFT}}{\rightleftharpoons}} F_r(f) = \tilde{a}_r(f) F_r(f), \quad (4.6.6)$$

$$\tilde{a}(f) = \int_{-\infty}^{\infty} \tilde{a}(x) \exp(i2\pi f x) dx = \sum_{k=-\infty}^{\infty} \hat{a}_{df}(k \Delta x) \exp(i2\pi k \Delta x f), \quad (4.6.7)$$

$$a_{df}(f) = a(f) F_d(f), \quad (4.6.8)$$

where

$$a(f) = \int_{-\infty}^{\infty} a(x) \exp(i2\pi f x) dx, \quad (4.6.9)$$

$$a_r(f) = \int_{-\infty}^{\infty} a_r(x) \exp(i2\pi f x) dx, \quad (4.6.10)$$

and

$$\tilde{a}_r(f) = \sum_{k=-\infty}^{\infty} \hat{a}_k \exp(i2\pi k f \Delta x) = \sum_{k=-\infty}^{\infty} \hat{a}_{df}(k \Delta x) \exp(i2\pi k \Delta x f), \quad (4.6.11)$$

are Fourier spectra of signals $a(x)$, $a_r(x)$ and $\tilde{a}_r(x)$ and

$$F_r(f) = \int_{-\infty}^{\infty} j_r(x) \exp(i2\pi f x) dx \quad (4.6.12)$$

and

$$F_d(f) = \int_{-\infty}^{\infty} j_d(x) \exp(i2\pi f x) dx \quad (4.6.13)$$

are, respectively, frequency responses of the signal/image reconstruction/display and discretization devices.

Consider now Eq. 4.6.7. Samples $a_{df}(k \Delta x)$ of signal $a_{df}(x)$ can be found from its spectrum $a_{df}(f)$ as:

$$a_{df}(k \Delta x) = \int_{-\infty}^{\infty} a_{df}(p) \exp(-i2\pi k \Delta x p) dp. \quad (4.6.14)$$

Then obtain:

$$\tilde{a}(f) = \sum_{k=-\infty}^{\infty} \int_{-\infty}^{\infty} a_{df}(p) \exp(-i2\pi k \Delta x p) dp \exp(i2\pi k \Delta x f) = \int_{-\infty}^{\infty} a_{df}(p) dp \sum_{k=-\infty}^{\infty} \exp[i2\pi k \Delta x (f - p)] \quad (4.6.15)$$

By Poisson's summation formula:

$$\sum_{k=-\infty}^{\infty} \exp[i2\pi k \Delta x (f - p)] = \Delta x \sum_{m=-\infty}^{\infty} \delta_{\xi} f - p + \frac{m \bar{0}}{\Delta x \bar{0}}. \quad (4.6.16)$$

Therefore,

$$\tilde{a}(f) = \Delta x \sum_{m=-\infty}^{\infty} a_{df} \left(f + \frac{m \bar{0}}{\Delta x \bar{0}} \right) \quad (4.6.17)$$

which means that sampling signal $a_{df}(x)$ results, in Fourier domain, in periodical replication of its spectrum with a period inverse to sampling interval Δx . This phenomenon is illustrated in Fig. 4-9.

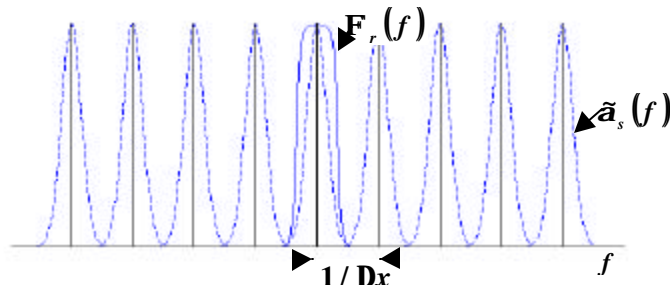


Figure 4-9. Illustration of Eq. (4.6.17) of periodical replication of signal spectrum in signal's sampled representation

In this interpretation, reconstruction of signal $a(x)$ is reduced, according to Eq. 4.6.5, to removing, from the set of periodically replicated copies $\{a_d(f + m/Df)\}$ of spectrum of signal $a_d(f)$ all extra replicas but the central $\{a_d(f)\}$ one by means of masking the set by frequency response $F_r(f)$ of the signal/image reconstruction device:

$$\begin{aligned} a(f) \circledast a_d(f) &= \tilde{a}_d(f) F_r(f) = \sum_{m=-\infty}^{\infty} \tilde{a}_d a_d \xi f + \frac{m \tilde{0}\tilde{u}}{Dx} F_r(f) = \\ &= \sum_{m=-\infty}^{\infty} \tilde{a}_d a_d \xi f + \frac{m \tilde{0}\tilde{u}}{Dx} F_r(f) + \frac{m \tilde{0}\tilde{u}}{Dx} F_r(f). \end{aligned} \quad (4.6.18)$$

From Eq. (4.6.18) one can easily see what type of signal distortions occur in the case of signal discretization by sampling. One can also see that perfect (distortion less) signal restoration from the result of its sampling is possible only if signals are band-limited:

$$a(f) = a_d(f) \text{rect}(fDx + 1/2) \quad (4.6.19)$$

and discretization and restoration devices act as ideal low-pass filters:

$$F_d(f) = \text{rect}(fDx + 1/2), \quad (4.6.20)$$

$$F_r(f) = \text{rect}(fDx + 1/2), \quad (4.6.21)$$

where

$$\text{rect}(x) = \begin{cases} 1, & 0 \leq x \leq 1 \\ 0, & \text{otherwise} \end{cases} \quad (4.6.22)$$

Eqs. (4.6.20-21) imply that:

$$j_d(x) = \frac{1}{Dx} \text{sinc}(px/Dx) \quad (4.6.23)$$

$$j_r(x) = \text{sinc}(px/Dx) \quad (4.6.24)$$

where $\text{sinc}(x) = \frac{\sin x}{x}$. In this ideal case

$$a(x) = \sum_{k=-\infty}^{\infty} \tilde{a}_k \text{sinc}[p(x - kDx)/Dx] \quad (4.6.25)$$

provided

$$\tilde{a}_k = \frac{1}{Dx} \int_{-\infty}^{\infty} \tilde{0}a(x) \text{sinc}[p(x - kDx)/Dx] dx = \int_{-\infty}^{\infty} \tilde{0}a(x) a(x - kDx) dx = a(kDx) \quad (4.6.26)$$

Eqs. (4.6.25 and 26) formulate *the sampling theorem*: band-limited signals can exactly reconstructed from their samples taken at the inter-sample distance that is inversely proportional to the signal bandwidth.

The above analyses resulted in the sampling theorem establishes also a link between the volume of the signal discrete representation, i.e., the number of signal samples N , and signal length X and signal spectral bandwidth F specified by the selected discretization interval Dx :

$$N = X/Dx = XF \quad (4.6.27)$$

Therefore *signal space-bandwidth product* XF is a fundamental parameter that defines signal degrees of freedom N .

4.6.2 Sampling 2-D and multidimensional signals

For sampling 2-D signals, 2-D discretization and restoration basis functions should be used. The simplest way to generate and to implement in image discretization and display devices 2-D discretization and restoration basis functions is to use separable 2-D basis functions that are formed as a product of 1-D function and that work separately in two dimensions when they are used for signal/image discretization and reconstruction:

$$\mathbf{j}_d^{2D}(x_1, x_2) = \mathbf{j}_d^{(1)}(x_1) \mathbf{j}_d^{(2)}(x_2); \mathbf{j}_r^{2D}(x_1, x_2) = \mathbf{j}_r^{(1)}(x_1) \mathbf{j}_r^{(2)}(x_2). \quad (4.6.28)$$

If 2-D separable basis functions are build from 1-D shift basis functions $\{\mathbf{j}_d^{(1)}(x_1 - kDx_1); \mathbf{j}_d^{(2)}(x_2 - kDx_2)\}$ and $\{\mathbf{j}_r^{(1)}(x_1 - kDx_1); \mathbf{j}_r^{(2)}(x_2 - kDx_2)\}$ 2-D signal sampling is carried out in sampling points arranged in a rectangular (Cartesian) raster which corresponds, in the domain of 2-D Fourier transform, to periodical replication of signal spectrum in Cartesian co-ordinates

as it is shown in Fig. 4-10. Yet another example of a periodical replication of image spectra in Cartesian coordinates is shown in Fig. 4-11(b).

One can see from these figures that the Cartesian periodical replication of 2-D signal spectrum does not necessarily ensures efficient spectra dense packing, and, correspondingly, least dense arrangement of signal sampling points for minimization of the volume of signal discrete representation. In general, tilted co-ordinate systems selected accordingly to the shape of the figure that encompasses signal 2-D spectrum will secure better spectra packing (Fig. 4-11 c,d). When sampling is carried out in a tilted coordinate system, sampling functions are not anymore separable functions of two Cartesian variables.

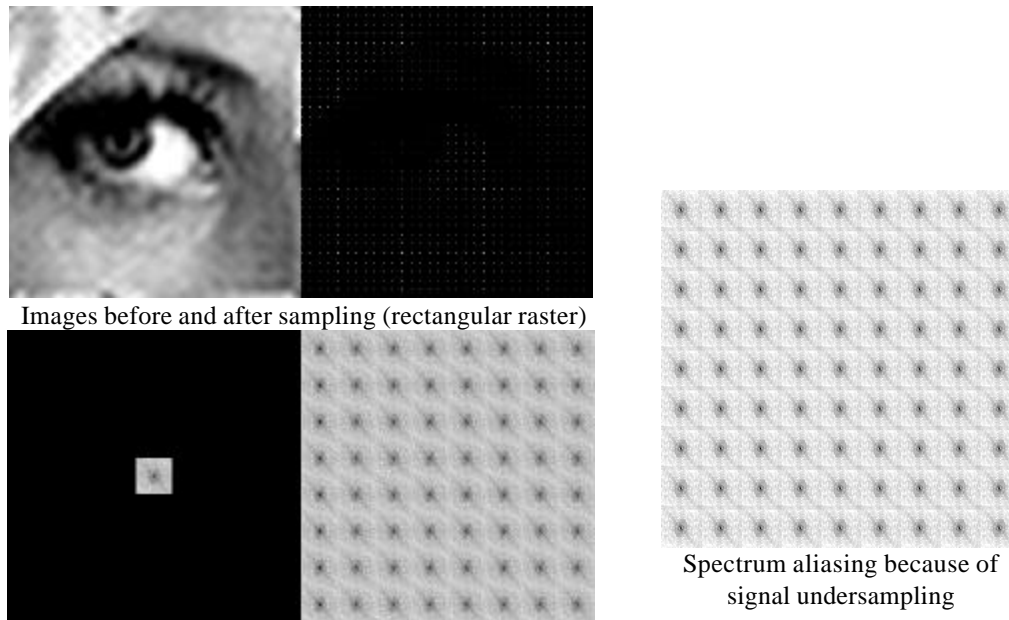


Figure 4-10. 2-D separable image sampling in a rectangular raster and periodical replication of its spectrum in a Cartesian co-ordinate system. Image at the bottom shows spectrum aliasing (seen as dark squares around main spectral lobes) that takes place when sampling interval is too large.

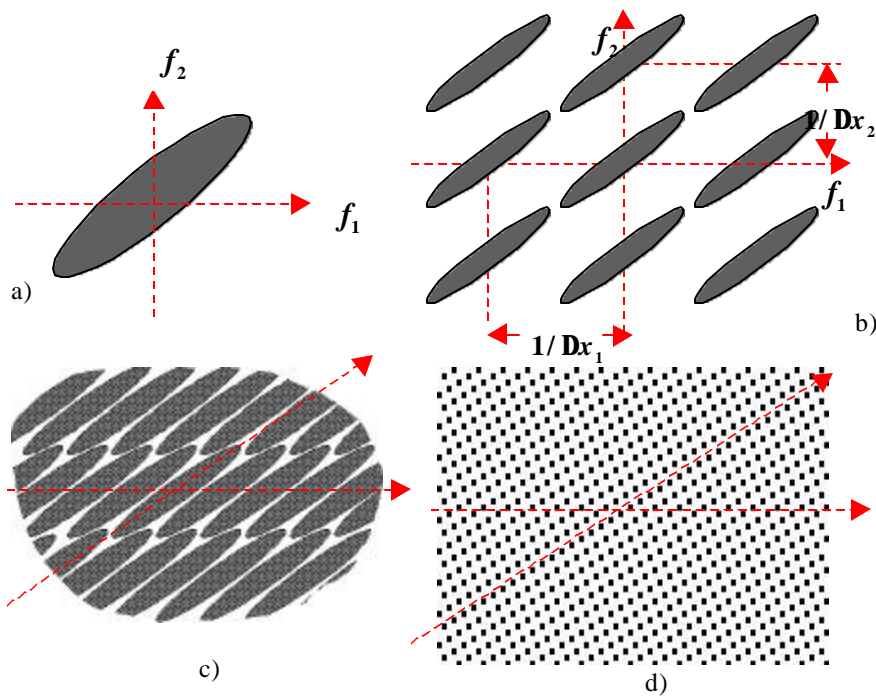


Figure 4-11. An example of an image spectrum (a), its periodical replication in rectangular (b) and tilted (c) coordinate systems and tilted discretization raster (d)

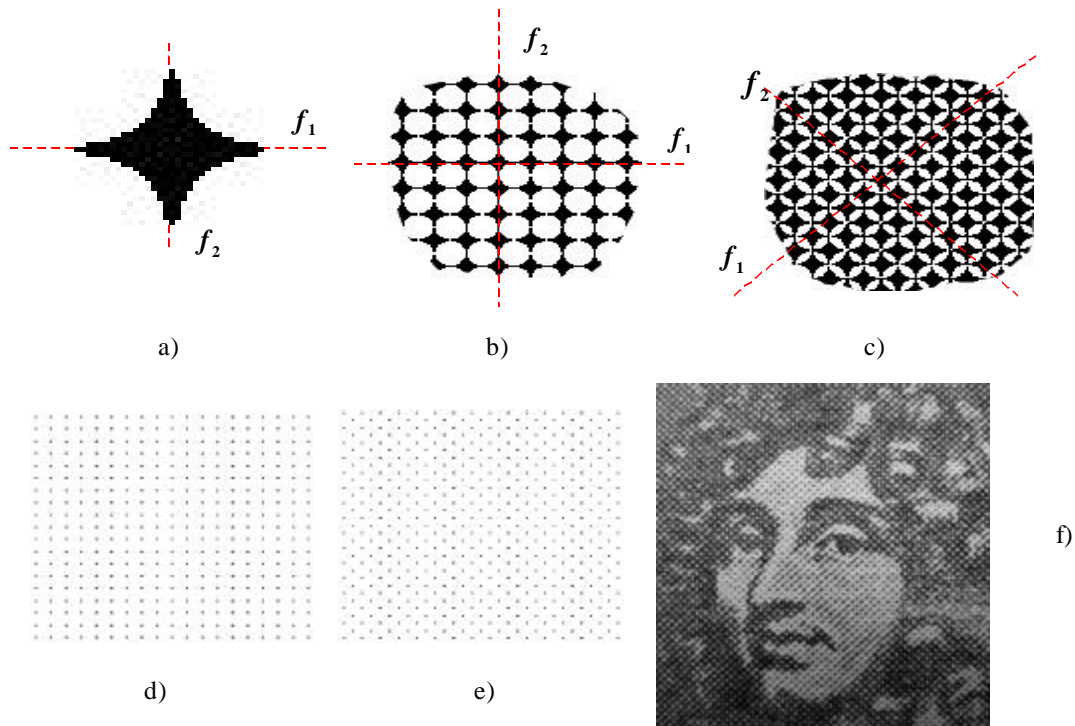


Figure 4-12 2-D sampling: a) figure in frequency domain that illustrates different sensitivity of human visual system to different spatial frequencies: higher for horizontal and vertical and lower for diagonal ones; b) , c) – periodical replication of the figure a) in a conventional and 45°-rotated rectangle coordinate systems, respectively; d), e) – corresponding image sampling rasters; f) an example of an image taken from a conventional book printing

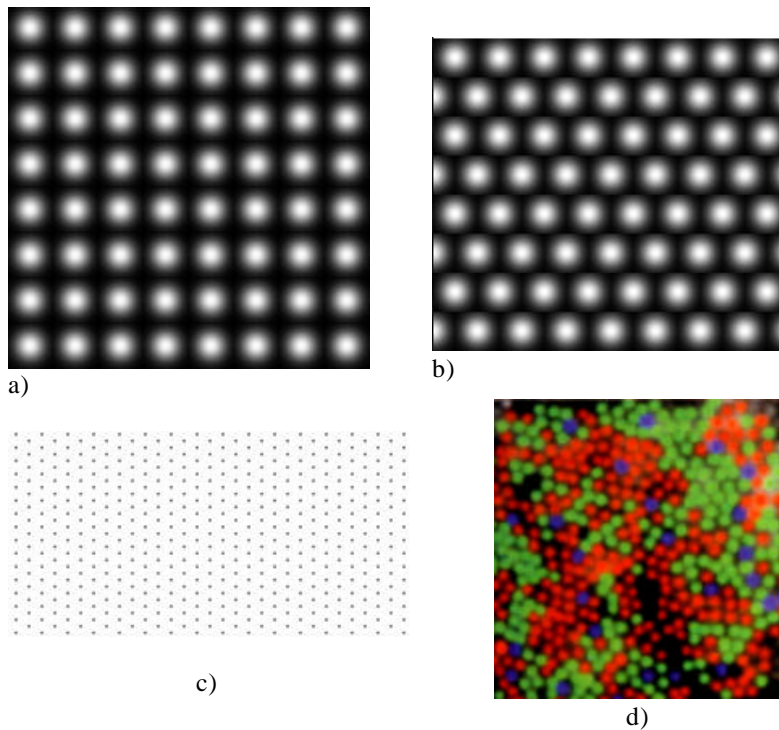


Figure 4-13. Image spectra replication for Cartesian (a) and hexagonal (b) sampling: the same number of circular spectra occupy less area when they are packed in a hexagonal co-ordinate system than in Cartesian co-ordinates; c) – hexagonal sampling raster; d) Trichromatic retinal mosaics: hexagonal arrangement of cones of human eye retina.

Rotating and tilting discretization rasters are not the only methods for the optimization of 2-D and multi dimensional sampling. Two other methods are “*discretization with gaps*” and *discretization with sub band decomposition*.

Method of the discretization with gaps is based on the use of signal spectra symmetry. It is illustrated in Fig. 4-14. Let signal spectrum is bounded as it is shown in Fig. 4-14 a). If one rotates the signal by 90° and superimposes the rotated copy onto the initial signal, a composite signal is obtained whose spectrum perfectly fills a square. Therefore, the composite signal can be optimally sampled in Cartesian co-ordinates. One can see that for all groups of four composite and initial signal samples centered around the rotation center, the following relationships hold:

$$z_1 = a_1 + a_4; z_2 = a_1 + a_2; z_3 = a_2 + a_3; z_4 = a_3 + a_4; \quad (4.6.29)$$

from which it follows that, from four samples $\{z_1, z_2, z_3, z_4\}$ of the composite signal one sample, say, z_4 , is redundant because it can be found from the other three ones:

$$z_4 = z_1 - z_2 + z_3. \quad (4.6.30)$$

Therefore the use of signal spectrum symmetry by means of sampling the composite signal obtained by superimposing the signal and its 90° rotated copy enables saving 25% of signal samples. Note, however, that the initial redundancy of signal spectrum (Fig. 4-14 (a)) is 50%.

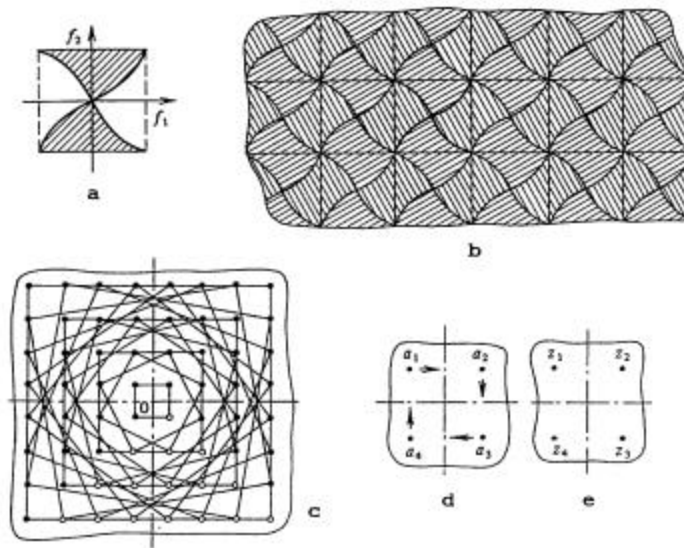


Figure 4-14. Discretization with gaps: a) – a figure bounding a signal spectrum (shaded); b) – the spectrum pattern obtained by superimposing the signal rotated by 90° and periodically extended in Cartesian co-ordinate system; c) the discretization raster corresponding to the spectrum's pattern (b); d) – group of four initial signal samples around the rotation center and directions of their translation after the rotation; e) – the corresponding group of four samples of the initial signal plus its 90° rotated copy. Empty circles in (c) denote redundant samples.

Method of discretization with sub-band decomposition is illustrated in Fig. 4-15. Area occupied by the signal spectrum is divided into sub-bands bounded by rectangles. Signals that correspond to sub-bands can then be optimally sampled in Cartesian rasters. For restoration of the initial signal, one should first restore, from their corresponding samples, sub-band signals and then add up them. Such a procedure allows, in principle, to achieve minimal volume of the signal discrete representation of

$N = S_{x_1, x_2} S_{f_1, f_2} = S_{x_1, x_2} \sum_k \dot{a} s_{f_1, f_2}^{(k)}$, where S_{x_1, x_2} and S_{f_1, f_2} are areas occupied, respectively, signal and its Fourier spectrum and summation over k assumes summation over sub-bands.

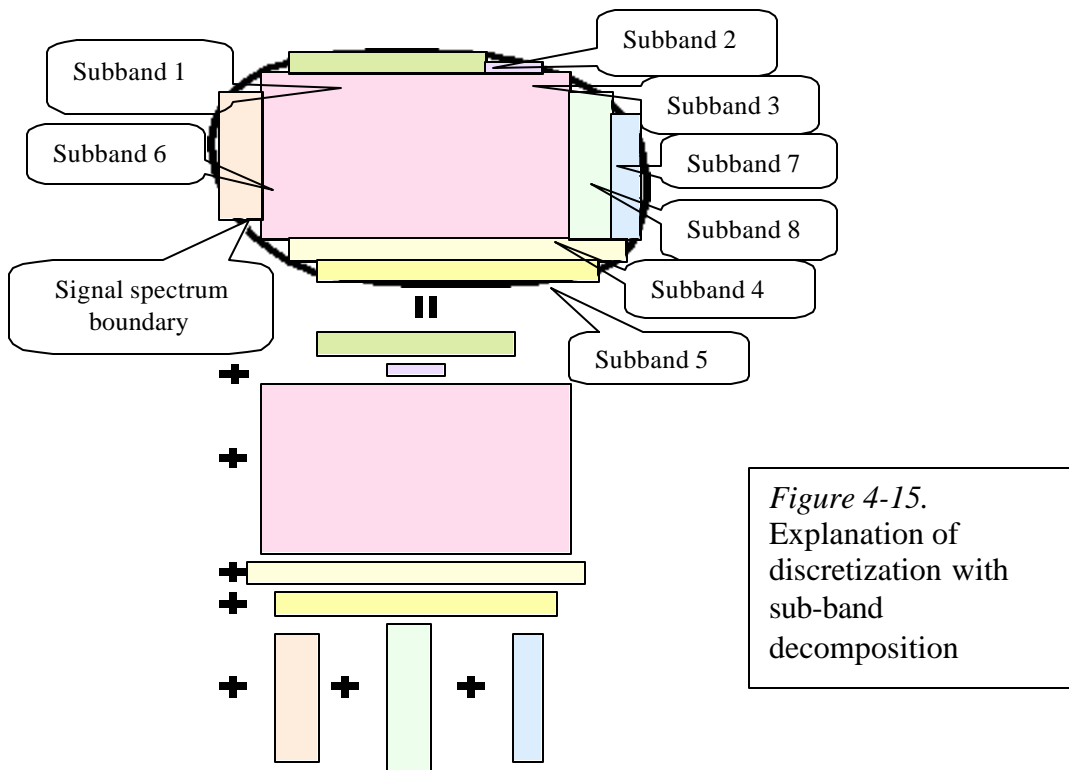
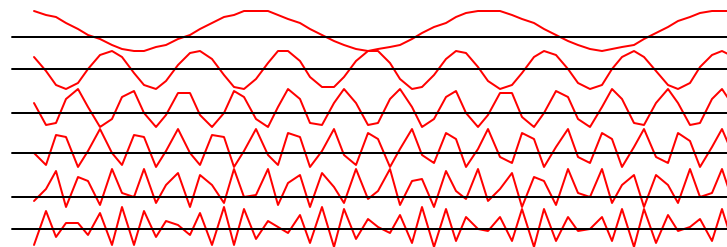


Figure 4-15. Explanation of discretization with sub-band decomposition

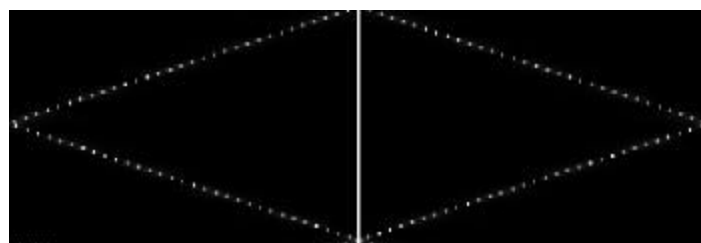
4.6.3 Sampling artifacts: qualitative analysis

As it is stated by the sampling theorem, signal sampling should be carried out after signal ideal low pass filtering in the bandwidth that corresponds to the selected sampling interval. Signal reconstruction from its samples also requires using ideal low pass filtering in the same bandwidth. In this case distortions because of signal sampling are minimal. Their mean squared value is equal to the energy of signal spectral components left outside of the chosen bandwidth. Real signal sampling and reconstruction devices are incapable of implementing the ideal low pass filtering. This causes additional distortions in reconstructed signals commonly called *aliasing effects*.

Two sources of aliasing effects should be distinguished: inappropriate signal pre-filtering for the sampling and inappropriate sampled signal low pass filtering for the reconstruction. Distortions caused by the former source are called *strobe effects*. They exhibit themselves as a stroboscopic reduction of frequency of signal components outside of the chosen bandwidth. Fig. 4-16 and 4-17 illustrate this phenomenon for 1-D and 2-D signals.



Signal spectra



Frequency

Figure 4-16. Strobe effects in sampling 1-D sinusoidal signals. Graphs on top show sinusoidal signals of different frequencies lower and higher the frequency that corresponds to the chosen discretization bandwidth. Image on bottom shows spectra (bright spots) of sampled sinusoidal signals of frequencies that increase from top to bottom. One can see that frequency of sampled sinusoids increases until it reaches the border of the bandwidth. After that the increase of signal frequency causes the decrease of the sampled signal frequency.

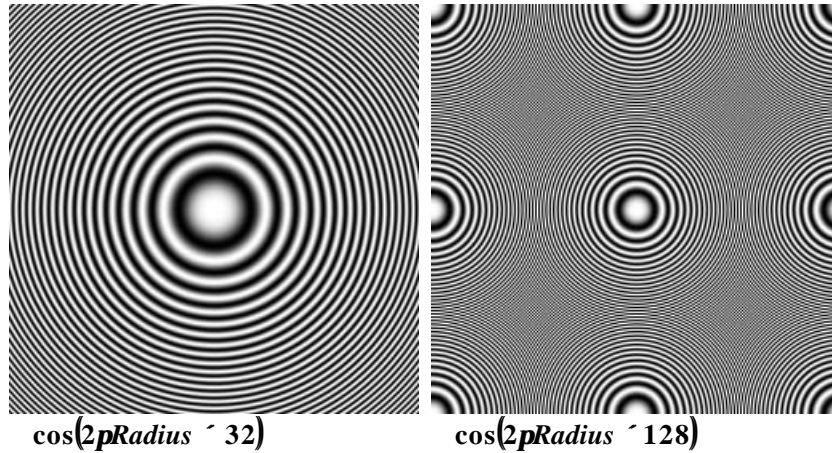


Figure 4-17. Strobe effects in sampling 2-D sinusoidal signals

Distortions caused by inappropriate sampled signal low pass filtering for the reconstruction exhibit themselves in appearance of signal high frequencies doubles from spectrum replicas not cleaned out by the reconstruction filter. For sinusoidal signals, their doubles cause low frequency beatings in the reconstructed signal that appear as moiré patterns. Owing to this reason, these aliasing effects are called *moiré effects*. In images, moiré effects usually appear in form of “pixelation” illustrated in Fig. 4-18.



Figure 4-18. Image “pixelation” effects caused by inappropriate reconstruction filtering

Numerical evaluation of aliasing effects in terms of mean squared signal reconstruction error can be carried out using Fourier Transform domain representation of sampling and reconstruction. However, mean squared reconstruction error is not always an adequate measure of the aliasing. For

instance, it does not directly evaluate such image quality feature as image readability. Fig. 4-19 illustrates importance of proper signal pre- and post-filtering in image sampling and reconstruction.

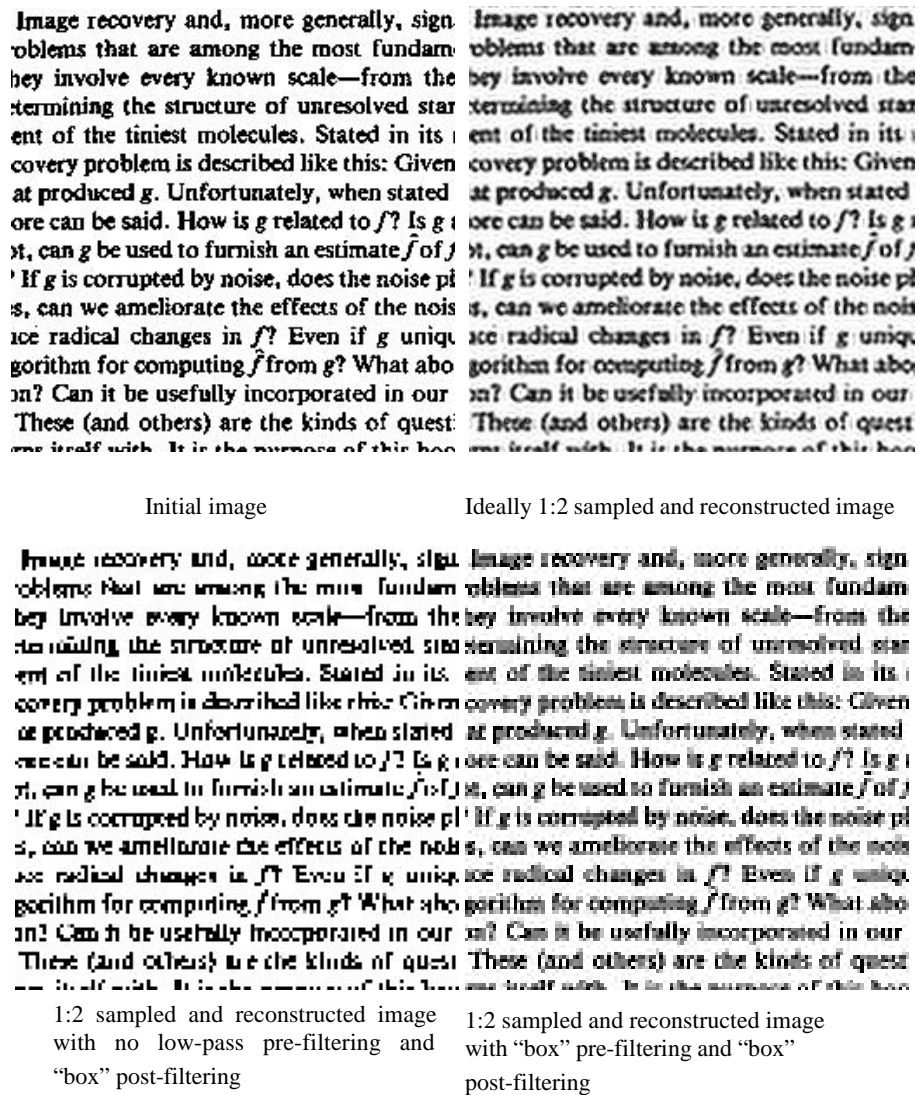


Figure 4-19. Influence of sampling artifacts on image readability: image sampling and reconstruction with an ideal low pass filter and with a "box" filter that computes signal average over a square box of 3x3 samples around each pixel.

4.6.4 Sampling artifacts: quantitative analysis

In this section, we will derive formulas that can be used for numerical evaluation of discretization artifacts. For the sake of simplicity, 1-D case will be analyzed. For 2-D signals, one should regard signal and spectral coordinate and indices as two-component vectors.

For discretization aperture $\mathbf{j}_d(\mathbf{x})$, sampling interval \mathbf{Dx} and signal reconstruction aperture $\mathbf{j}_r(\mathbf{x})$, signal samples at points $\{(k + u)\mathbf{Dx}\}$, where $u\mathbf{Dx}$ is a shift in positioning discretization aperture with respect to signal coordinate system \mathbf{x} , are measured as (Eq. 4.6.1a):

$$a_k = \frac{1}{\mathbf{Dx}} \int_{-\mathbf{X}}^{\mathbf{X}} \dot{\mathbf{a}}(\mathbf{x}) \mathbf{j}_d[\mathbf{x} - (k + u)\mathbf{Dx}] d\mathbf{x} = \frac{1}{\mathbf{Dx}} \int_{-\mathbf{X}}^{\mathbf{X}} \dot{\mathbf{a}}(\mathbf{x}) \dot{\mathbf{a}}(\mathbf{x}) \mathbf{j}_d(\mathbf{x} - \mathbf{x}) d\mathbf{x} \frac{\bar{\mathbf{u}}}{\mathbf{p}} d[\mathbf{x} - (k + u)\mathbf{Dx}] d\mathbf{x} = \frac{1}{\mathbf{Dx}} \int_{-\mathbf{X}}^{\mathbf{X}} \dot{\mathbf{a}}_{df}(\mathbf{x}) d[\mathbf{x} - (k + u)\mathbf{Dx}] d\mathbf{x}, \quad (4.6.31)$$

where

$$a_{df}(\mathbf{x}) = \int_{-\mathbf{X}}^{\mathbf{X}} \dot{\mathbf{a}}(\mathbf{x}) \mathbf{j}_d(\mathbf{x} - \mathbf{x}) d\mathbf{x} \quad (4.6.32)$$

(see Fig. 3-10) and reconstructed signal is generated as

$$a_r(\mathbf{x}) = \int_{k=-N}^N \dot{\mathbf{a}}_k \mathbf{j}_r[\mathbf{x} - (k + v)\mathbf{Dx}] d\mathbf{x} \quad (4.6.33)$$

where $2N + 1$ is the number of samples used for the reconstruction and $v\mathbf{Dx}$ is shift of the reconstruction aperture with respect to the signal coordinate system.

Find an explicit relationship between $\mathbf{a}(\mathbf{x})$ and $\mathbf{a}_r(\mathbf{x})$ that involves discretization and reconstruction device parameters:

$$\mathbf{a}_r(\mathbf{x}) = \int_{k=-N}^N \dot{\mathbf{a}}_k \mathbf{j}_r[\mathbf{x} - (k + v)\mathbf{Dx}] d\mathbf{x} = \frac{1}{\mathbf{Dx}} \int_{k=-N}^N \int_{-\mathbf{X}}^{\mathbf{X}} \dot{\mathbf{a}}(\mathbf{x}) \mathbf{j}_d[\mathbf{x} - (k + u)\mathbf{Dx}] d\mathbf{x} \frac{\bar{\mathbf{u}}}{\mathbf{p}} \mathbf{j}_r[\mathbf{x} - (k + v)\mathbf{Dx}] d\mathbf{x} = \frac{1}{\mathbf{Dx}} \int_{-\mathbf{X}}^{\mathbf{X}} \dot{\mathbf{a}}(\mathbf{x}) d\mathbf{x} \int_{k=-N}^N \dot{\mathbf{a}}_k \mathbf{j}_d[\mathbf{x} - (k + u)\mathbf{Dx}] \mathbf{j}_r[\mathbf{x} - (k + v)\mathbf{Dx}] d\mathbf{x} = \int_{-\mathbf{X}}^{\mathbf{X}} \dot{\mathbf{a}}(\mathbf{x}) h(\mathbf{x}, \mathbf{x}) d\mathbf{x}, \quad (4.6.34)$$

where

$$h(\mathbf{x}, \mathbf{x}) = \frac{1}{\mathbf{Dx}} \int_{k=-N}^N \dot{\mathbf{a}}_k \mathbf{j}_d[\mathbf{x} - (k + u)\mathbf{Dx}] \mathbf{j}_r[\mathbf{x} - (k + v)\mathbf{Dx}] d\mathbf{x} \quad (4.6.35)$$

is an equivalent impulse response of the discretization/reconstruction procedure.

As we saw it in Sect. 4.6.1, it is easier to analyze sampling artifacts in signal Fourier domain. Find Fourier spectrum $\mathbf{a}(f)$ of the reconstructed signal and connect it with spectrum $\mathbf{a}(f)$ of the initial signal:

$$\begin{aligned} \mathbf{a}(f) &= \int_{-\mathbf{X}}^{\mathbf{X}} \dot{\mathbf{a}}_r(\mathbf{x}) \exp(i2\mathbf{p}\mathbf{x}) d\mathbf{x} = \int_{-\mathbf{X}}^{\mathbf{X}} \int_{-\mathbf{X}}^{\mathbf{X}} \dot{\mathbf{a}}(\mathbf{x}) h(\mathbf{x}, \mathbf{x}) d\mathbf{x} \frac{\bar{\mathbf{u}}}{\mathbf{p}} \exp(i2\mathbf{p}\mathbf{x}) d\mathbf{x} = \\ &= \int_{-\mathbf{X}}^{\mathbf{X}} \int_{-\mathbf{X}}^{\mathbf{X}} \dot{\mathbf{a}}(\mathbf{x}) \dot{\mathbf{a}}(\mathbf{p}) \exp(-i2\mathbf{p}\mathbf{x}) d\mathbf{p} \frac{\bar{\mathbf{u}}}{\mathbf{p}} h(\mathbf{x}, \mathbf{x}) \exp(i2\mathbf{p}\mathbf{x}) d\mathbf{x} d\mathbf{x} = \\ &= \int_{-\mathbf{X}}^{\mathbf{X}} \dot{\mathbf{a}}(\mathbf{p}) d\mathbf{p} \int_{-\mathbf{X}}^{\mathbf{X}} \dot{\mathbf{a}} h(\mathbf{x}, \mathbf{x}) \exp[i2\mathbf{p}(f\mathbf{x} - \mathbf{p}\mathbf{x})] \exp(-i2\mathbf{p}\mathbf{x}) d\mathbf{p} d\mathbf{x} d\mathbf{x} = \int_{-\mathbf{X}}^{\mathbf{X}} \dot{\mathbf{a}}(\mathbf{p}) H(f, \mathbf{p}) d\mathbf{p}, \end{aligned} \quad (4.6.36)$$

where $H(f, \mathbf{p})$ is a frequency response of the sampling/reconstruction procedure:

$$\begin{aligned} H(f, \mathbf{p}) &= \int_{-\mathbf{X}}^{\mathbf{X}} \dot{\mathbf{a}} h(\mathbf{x}, \mathbf{x}) \exp[i2\mathbf{p}(f\mathbf{x} - \mathbf{p}\mathbf{x})] d\mathbf{x} d\mathbf{x} = \\ &= \frac{1}{\mathbf{Dx}} \int_{-\mathbf{X}}^{\mathbf{X}} \int_{-\mathbf{X}}^{\mathbf{X}} \dot{\mathbf{a}} \dot{\mathbf{a}}_k \mathbf{j}_d[\mathbf{x} - (k + u)\mathbf{Dx}] \mathbf{j}_r[\mathbf{x} - (k + v)\mathbf{Dx}] \exp[i2\mathbf{p}(f\mathbf{x} - \mathbf{p}\mathbf{x})] d\mathbf{x} d\mathbf{x} = \\ &= \frac{1}{\mathbf{Dx}} \int_{k=-N}^N \int_{-\mathbf{X}}^{\mathbf{X}} \dot{\mathbf{a}} \dot{\mathbf{a}}_k \mathbf{j}_d[\mathbf{x} - (k + u)\mathbf{Dx}] \mathbf{j}_r[\mathbf{x} - (k + v)\mathbf{Dx}] \exp[i2\mathbf{p}(f\mathbf{x} - \mathbf{p}\mathbf{x})] d\mathbf{x} d\mathbf{x} = \\ &= \frac{1}{\mathbf{Dx}} \int_{k=-N}^N \int_{-\mathbf{X}}^{\mathbf{X}} \dot{\mathbf{a}} \dot{\mathbf{a}}_k [\mathbf{x} - (k + u)\mathbf{Dx}] \exp(-i2\mathbf{p}\mathbf{x}) d\mathbf{x} \dot{\mathbf{a}}_k [\mathbf{x} - (k + v)\mathbf{Dx}] \exp(i2\mathbf{p}\mathbf{x}) d\mathbf{x} = \\ &= \frac{1}{\mathbf{Dx}} \int_{k=-N}^N \dot{\mathbf{a}} \dot{\mathbf{a}}_k(\tilde{\mathbf{x}}) \exp\{-i2\mathbf{p}[\tilde{\mathbf{x}} + (k + u)\mathbf{Dx}]\} d\tilde{\mathbf{x}} \dot{\mathbf{a}}_k(\tilde{\mathbf{x}}) \exp\{i2\mathbf{p}[\tilde{\mathbf{x}} + (k + v)\mathbf{Dx}]\} d\tilde{\mathbf{x}} = \end{aligned}$$

$$\frac{1}{Dx} \sum_{k=-\infty}^{\infty} \dot{\mathbf{a}} \exp[-i2\mathbf{p}(k+u)Dx] \exp[i2\mathbf{p}(k+v)Dx] \sum_{\tilde{x}=-\infty}^{\infty} \dot{\mathbf{j}}_d(\tilde{x}) \exp(-i2\mathbf{p}\tilde{x}) \dot{\mathbf{j}}_r(\tilde{x}) \exp(i2\mathbf{p}\tilde{x}) d\tilde{x} = \frac{\mathbf{F}_d^*(p) \star \mathbf{F}_r(f)}{Dx} \exp[i2\mathbf{p}(fv-pu)Dx] \star \sum_{k=-N}^N \dot{\mathbf{a}} \exp[i2\mathbf{p}(f-p)kDx], \quad (4.6.37)$$

where $\mathbf{F}_d(\cdot)$ and $\mathbf{F}_r(\cdot)$ are frequency responses of signal discretization and reconstruction devices.

Consider the summation term in Eq. (4.6.37):

$$\sum_{k=-N}^N \dot{\mathbf{a}} \exp[i2\mathbf{p}(f-p)kDx] = \frac{\exp[i2\mathbf{p}(f-p)(N+1)Dx] - \exp[-i2\mathbf{p}(f-p)NDx]}{\exp[i2\mathbf{p}(f-p)Dx] - 1} = \frac{\sin[\mathbf{p}(f-p)(2N+1)Dx]}{\sin[\mathbf{p}(f-p)Dx]} = (2N+1) \frac{\sin[\mathbf{p}(f-p)(2N+1)Dx]}{(2N+1)\sin[\mathbf{p}(f-p)Dx]}. \quad (4.6.38)$$

Using Eq. 4.6.38, overall frequency response of the signal discretization-reconstruction procedure can be written as

$$H(f, p) = \exp[i2\mathbf{p}(fv-pu)Dx] \star \mathbf{F}_d^*(p) \star \mathbf{F}_r(f) \frac{(2N+1) \sin[\mathbf{p}(f-p)(2N+1)Dx]}{Dx (2N+1)\sin[\mathbf{p}(f-p)Dx]}. \quad (4.6.39)$$

This equation shows that the signal discretization/reconstruction procedure being implemented by shift basis function is nevertheless not shift invariant for shift invariant system with PSF $h(\mathbf{x}, \mathbf{x}) = h(\mathbf{x} - \mathbf{x})$ frequency response has a form $H(f, p) = H(f) \mathbf{d}(f - p)$. The reason of space variance is finite number of signal samples used for the reconstruction, or, in other words, boundary effects. When this number increases boundary effects can be neglected. Therefore consider asymptotic behavior of $H(f, p)$ when $N \rightarrow \infty$.

By Poisson's summation formula:

$$\lim_{N \rightarrow \infty} \sum_{k=-\infty}^{\infty} \dot{\mathbf{a}} \exp[i2\mathbf{p}kDx(f-p)] = Dx \sum_{m=-\infty}^{\infty} \dot{\mathbf{a}} \dot{\mathbf{c}}_{\xi}^{\mathbf{a}} f - p + \frac{m \bar{0}}{Dx \mathbf{g}}, \quad (4.6.40)$$

obtain from Eq. 4.6.35:

$$\lim_{N \rightarrow \infty} H(f, p) = \exp[i2\mathbf{p}(fv-pu)Dx] \star \mathbf{F}_d^*(p) \star \mathbf{F}_r(f) Dx \sum_{m=-\infty}^{\infty} \dot{\mathbf{a}} \dot{\mathbf{c}}_{\xi}^{\mathbf{a}} f - p + \frac{m \bar{0}}{Dx \mathbf{g}}. \quad (4.6.41)$$

Substitution of Eq. 4.6.41 into Eq. 4.6.37 then gives:

$$\begin{aligned} \lim_{N \rightarrow \infty} \mathbf{a}_r(f) &= \sum_{\tilde{x}=-\infty}^{\infty} \dot{\mathbf{a}}(\tilde{x}) \exp[i2\mathbf{p}(fv-pu)Dx] \star \mathbf{F}_d^*(p) \star \mathbf{F}_r(f) \sum_{m=-\infty}^{\infty} \dot{\mathbf{a}} \dot{\mathbf{c}}_{\xi}^{\mathbf{a}} f - p + \frac{m \bar{0}}{Dx \mathbf{g}} dp = \\ & \mathbf{F}_r(f) \exp[i2\mathbf{p}(u-v)Dx] \sum_{m=-\infty}^{\infty} \dot{\mathbf{a}} \dot{\mathbf{c}}_{\xi}^{\mathbf{a}} f + \frac{m \bar{0}}{Dx \mathbf{g}} \exp \frac{\mathbf{x}}{\xi} - i2\mathbf{p} \frac{mu \bar{0}}{Dx \mathbf{g}} \star \mathbf{F}_d^* \dot{\mathbf{c}}_{\xi}^{\mathbf{a}} f + \frac{m \bar{0}}{Dx \mathbf{g}} = \\ & \mathbf{F}_r(f) \mathbf{F}_d^*(f) \mathbf{a}(f) \exp[i2\mathbf{p}(u-v)Dx] + \mathbf{F}_r(f) \exp[i2\mathbf{p}(u-v)Dx] \cdot \\ & \sum_{m=\bar{e}}^{\infty} \dot{\mathbf{a}} \dot{\mathbf{c}}_{\xi}^{\mathbf{a}} \dot{\mathbf{c}}_{\xi}^{\mathbf{a}} f + \frac{m \bar{0}}{Dx \mathbf{g}} \exp \frac{\mathbf{x}}{\xi} - i2\mathbf{p} \frac{mu \bar{0}}{Dx \mathbf{g}} + \mathbf{a}_{df} \dot{\mathbf{c}}_{\xi}^{\mathbf{a}} f - \frac{m \bar{0}}{Dx \mathbf{g}} \exp \frac{\mathbf{x}}{\xi} i2\mathbf{p} \frac{mu \bar{0}}{Dx \mathbf{g}}. \end{aligned} \quad (4.6.43)$$

One can interpret Eq. 4.6.43 as one showing that the signal $\mathbf{a}_r(\mathbf{x})$ reconstructed from samples $\{\mathbf{a}_k\}$ of signal $\mathbf{a}(\mathbf{x})$ consists of 2 components. The first component is a copy of signal $\mathbf{a}(\mathbf{x})$, shifted by $(u-v)Dx$ and modified by convolution with point spread functions of the discretization and reconstruction devices. Its spectrum is described by the first term of Eq. 4.6.41. The second component is aliasing one. Its spectrum is described by the second term of Eq. 4.6.41. It consists of periodical

replicas $\sum_{\bar{e}}^{\infty} \dot{\mathbf{a}} \dot{\mathbf{c}}_{\xi}^{\mathbf{a}} \dot{\mathbf{c}}_{\xi}^{\mathbf{a}} f \pm \frac{m \bar{0}}{Dx \mathbf{g}} \exp \frac{\mathbf{x}}{\xi} + i2\mathbf{p} \frac{mu \bar{0}}{Dx \mathbf{g}}$ spectrum $\mathbf{a}_{df}(f)$ of signal $\mathbf{a}_{df}(\mathbf{x})$ (Eq. 4.6.32).

In the numerical evaluation of signal distortions caused by the discretization/reconstruction, it is devisable to distinguish two types of distortions that are described by the above two reconstructed signal components: distortions owing to the signal blur by the discretization and reconstruction apertures and aliasing distortions. The former are completely specified by deviation of reconstructed signal spectrum from the initial one:

$$\mathbf{e}_{sp}(f) = [1 - \mathbf{F}_r(f) \mathbf{F}_d^*(f)] \mathbf{a}(f) \quad (4.6.44)$$

(note that shift factor $\exp[i2\pi(u-v)\mathbf{D}\mathbf{x}]$ in the evaluation of this error can be neglected as irrelevant).

For the evaluation of the second type of distortions, the most straightforward measure is that of its energy which, by Parseval theorem, is

$$\overline{e_d^2} = \int_{-\infty}^{\infty} e_d^2(f) df, \quad (4.6.45)$$

where

$$e_d^2(f) = |F_r(f)|^2 \sum_{m=1}^{\infty} \left| \mathbf{a}_{\mathbf{e}}^T f + \frac{m \cdot \mathbf{0}}{\mathbf{D}\mathbf{x}} \right|^2 \left| F_d \mathbf{a}_{\mathbf{e}}^T f + \frac{m \cdot \mathbf{0}}{\mathbf{D}\mathbf{x}} \right|^2 + \sum_{m=1}^{\infty} \left| \mathbf{a}_{\mathbf{e}}^T f - \frac{m \cdot \mathbf{0}}{\mathbf{D}\mathbf{x}} \right|^2 \left| F_d \mathbf{a}_{\mathbf{e}}^T f - \frac{m \cdot \mathbf{0}}{\mathbf{D}\mathbf{x}} \right|^2. \quad (4.6.46)$$

For image spectra usually decay with frequency, the value

$$\overline{e_d^2} = \int_{-\infty}^{\infty} |F_r(f)|^2 \sum_{m=1}^{\infty} \left| \mathbf{a}_{\mathbf{e}}^T f + \frac{m \cdot \mathbf{0}}{\mathbf{D}\mathbf{x}} \right|^2 + \left| \mathbf{a}_{\mathbf{e}}^T f - \frac{m \cdot \mathbf{0}}{\mathbf{D}\mathbf{x}} \right|^2 df \quad (4.6.47)$$

can be used as an upper bound of aliasing error.

4.6.5 Multi-resolution sampling

The idea of optimal sampling with sub-band decomposition described in Sect. 4.6.2 has found its implementation in multi-resolution sampling that gained its popularity under the name of wavelet decomposition. Multi-resolution sampling can be most easily explained for 1-D signals. As it is illustrated in Fig. 3-24, signal is split into two components, low pass and high pass ones. The low pass component has bandwidth half of that of the initial signal and can be sampled with half of the sampling rate of the initial signal. The residual high pass component's spectrum bandwidth is also half of the initial bandwidth but its spectral components are situated in the upper half of the spectral range. Therefore, in order to sample it with half of the initial sampling rate one should shift its spectrum into the lower half of the range.

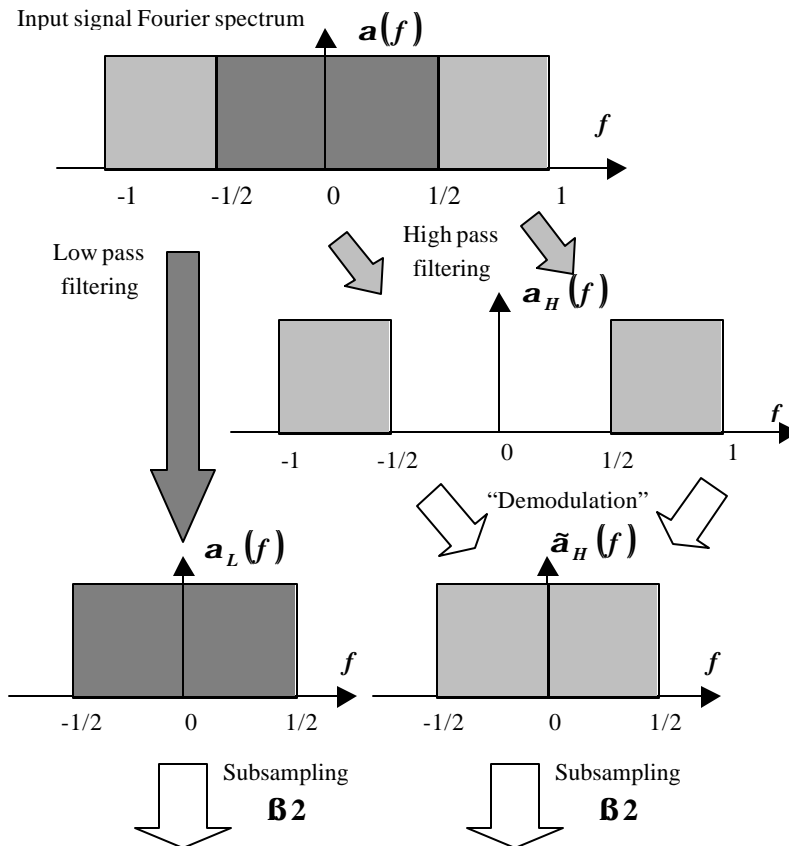


Figure 4-20. Multi-resolution sampling explained for a 1-D signal in Fourier domain

This is achieved by means of its “demodulation” which is implemented by multiplying the “high pass” signal component by a sinusoidal signal whose frequency is equal to half of the initial signal highest frequency. In multi-resolution sampling, this procedure is repeated recursively to “low pass” components obtained on each previous step of the recursion as it is shown in Fig. 4-21.

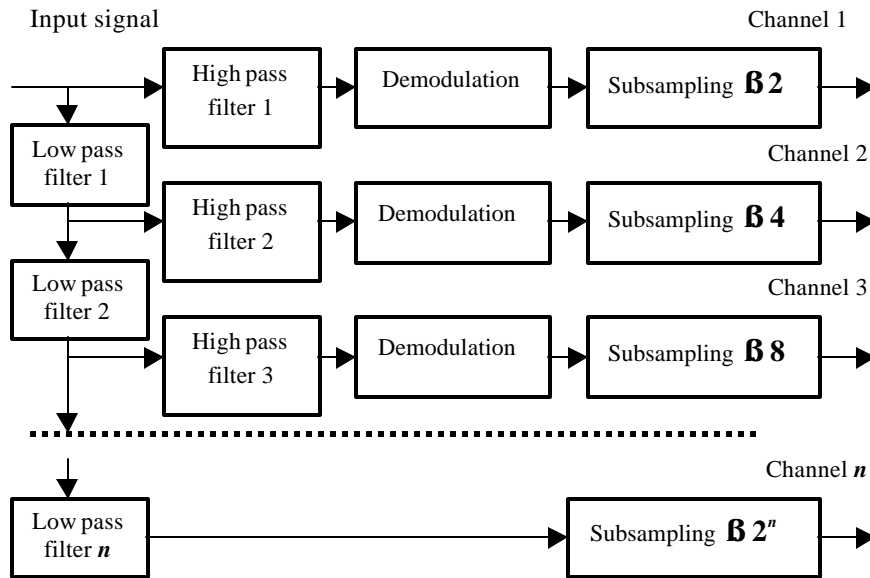


Figure 4-21. Multi resolution signal sampling flow diagram

On each step, bandwidths of low pass and high pass filters, and therefore signal sampling rate are half of those on the previous step. On the last n -th step, low pass component obtained on this stage has bandwidth equal to $1/2^n$ -th fraction of the initial signal bandwidth and it is sampled accordingly with $1/2^n$ -th of the rate that corresponds to this initial bandwidth. Signal reconstruction from its multi resolution sampled representation is also carried out component (channel) wise. Each sampled high pass component is reconstructed individually accordingly to its bandwidth and its spectrum is shifted correspondingly and then all reconstructed components are added up to form the entire reconstructed signal.

Obviously, the described multi resolution sampling does not reduce the number of signal samples with respect to that corresponding to the signal bandwidth. It however enables applying different quantization to different signal components and in this way to gain in the final volume of signal digital representation. The method has found its application in wavelet image coding.